Graphene Materials

DOI: 10.1002/ange.201303497

3D Honeycomb-Like Structured Graphene and Its High Efficiency as a Counter-Electrode Catalyst for Dye-Sensitized Solar Cells**

*Hui Wang, Kai Sun, Franklin Tao, Dario J. Stacchiola, and Yun Hang Hu**

Graphene, a two-dimensional carbon sheet,[1] has attracted great interest due to its unique properties.[2,3] To explore its practical applications, large-scale synthesis with controllable integration of individual graphene sheets is essential. To date, numerous approaches have been developed for graphene synthesis, including mechanical cleavage,[1] epitaxial growth,[4] and chemical vapor deposition.[5] All of those techniques are used to prepare flat graphene sheets on a substrate. Chemical exfoliation of graphite has been applied to prepare graphene oxide solutions and graphene-based composite materials.[6,7] Recently, tuning graphene shapes is attracting much attention.[8–16] Cheng and co-workers synthesized graphene foam using porous Ni foam as a template for the CVD growth of graphene, followed by etching away the Ni skeleton.[8] The graphene foam consists of an interconnected flexible network of graphene as the fast transport channel of charge carriers for high electrical conductivity. Ruoff et al. prepared porous graphene paper from microwave exfoliated graphene oxide by KOH activation.[9] The porous graphene, which has an ultra-high surface area and a high electrical conductivity, was exploited for supercapacitor cells, leading to high values of gravimetric capacitance and energy density. Feng, Müllen, and co-workers synthesized hierarchical macro- and mesoporous graphene frameworks (GFs).[10–12] The GFs exhibited excellent performance for electrochemical capacitive energy storage. Yu et al.[13] and Qu et al.[14] fabricated graphene tubes that could be selectively functionalized for desirable applications. Choi et al. synthesized macroporous graphene using polystyrene colloidal particles as sacrificial templates in graphene oxide suspension,[15] and the pore sizes can be tuned by controlling template particle size.[16] These important results represent a significant topic—tuning the properties of graphene sheets by controlling their shapes. However, it is still a challenge to synthesize three-dimensional graphene (3D) with a desirable shape.

Herein, we develop a novel strategy for the synthesis of a new type of graphene sheet with a 3D honeycomb-like structure by a simple reaction between Li_2O and CO. Furthermore, these graphene sheets exhibited excellent catalytic performance as a counter electrode for dye-sensitized solar cells (DSSCs) with an energy conversion efficiency as high as 7.8%, which is comparable to that of an expensive platinum electrode.

Li_2O is widely exploited as a promoter in catalysts to inhibit carbon formation.[17] However, this general principle is challenged by this work, in which Li_2O is used to react with CO to form graphene-structured carbon [Eq. (1)]

$$Li_2O + 2\,CO \rightarrow C(\text{graphene}) + Li_2CO_3 \quad (1)$$

This strategy is supported by our thermodynamic calculations: The Gibbs free energy change is negative, indicating that this reaction is thermodynamically favorable (Figure S1 in the Supporting Information). The negative enthalpy change ($\Delta H_{298} = -397.5\ kJ\,mol^{-1}$) suggests it is an energy-economic process. Furthermore, simultaneous formation of Li_2CO_3 with graphene can isolate the graphene sheets from each other to prevent graphite formation during the process. On the other hand, the Li_2CO_3 particles will also play a role in determining the locally curved shape of the graphene sheets. The feasibility of this novel approach was confirmed by following experiments.

1 mol of lithium oxide (Li_2O) powder (from Aldrich) was treated with CO in a batch ceramic-tube reactor at an initial pressure of 35 psi and temperature of 550 °C for 12, 24, or 48 h. The products were subjected to X-ray diffraction (XRD) measurements. As shown in Figure 1, diffraction peaks for Li_2CO_3 can be observed, confirming the reaction between Li_2O and CO. The conversions of Li_2O are 87, 90, and 92% for 12, 24, and 48 h, respectively. The average crystal size of Li_2CO_3 is 40 nm. The products were treated with hydrochloric acid to remove Li_2O and Li_2CO_3, then washed with H_2O, and dried at 80 °C, the black powder was obtained and identified as carbon by elementary analysis. Surface areas are 151, 153, and 128 $m^2\,g^{-1}$ for the carbon samples prepared with 12, 24, and 48 h, respectively. Their pore sizes are mostly in the range from 115 to 170 nm.

Field emission scanning electron microscopy (FESEM) was employed to evaluate the structure of the carbon powder.

[*] H. Wang, Prof. Y. H. Hu
Department of Materials Science and Engineering
Michigan Technological University
1400 Townsend Drive, Houghton, MI 49931-1295 (USA)
E-mail: yunhangh@mtu.edu
Dr. K. Sun
Department of Materials Science and Engineering
University of Michigan
Ann Arbor, MI 48109-2136 (USA)
Prof. F. Tao
Department of Chemistry and Biochemistry
University of Notre Dame
Notre Dame, IN 46556 (USA)
Dr. D. J. Stacchiola
Chemistry Department, Brookhaven National Laboratory
Upton, NY 11973 (USA)

[**] This work was partially supported by the U.S. National Science Foundation (NSF-CBET-0931587) and the ACS Petroleum Research Fund (PRF-51799-ND10).

Supporting information for this article is available on the WWW under http://dx.doi.org/10.1002/anie.201303497.

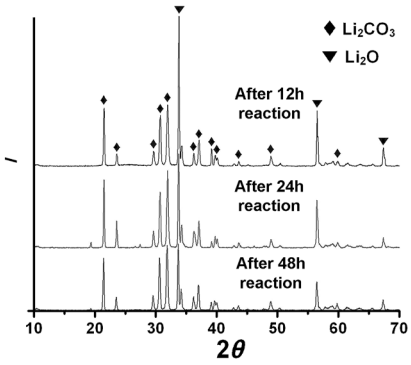

Figure 1. XRD patterns of solid products from the reaction between Li_2O and CO at 550 °C.

As shown in Figure 2 a and b, the graphene sheets are curved with thickness of about 2 nm, and connect to each other and form a 3D honeycomb-like structure. The cell size of graphene honeycombs lies in the range of 50–500 nm. The

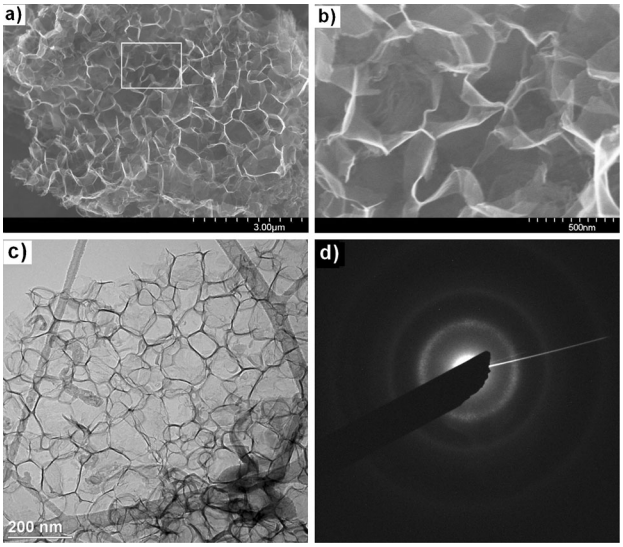

Figure 2. FESEM and TEM images of honeycomb-structured graphene (HSG). a) FESEM image, b) enlarged FESEM image for the marked square area in (a), c) TEM image, and d) electron diffraction pattern.

micro-structure of honeycomb cells was further evaluated by transmission electron microscopy (TEM). The TEM image showed the intrinsic wrinkles or corrugations of the cell sheets (Figure 2 c). Furthermore, the curved shapes of honeycomb-structured graphene (HSG) were further supported by electron diffraction that shows poly-crystalline ring patterns (Figure 2 d). Different from spot patterns of flat graphene sheets,[18,19] ring diffraction patterns arise from scrolled or folded graphene sheets.[18] In addition, electron energy loss spectroscopy (EELS) was used to investigate the local structure of HSG sheets. As shown in Figure 3 a and b, for all four selected locations, an intensive feature of sp^2 bonded carbon atoms in the carbon K-edge region is seen: a peak at 285 eV corresponding to the 1s-π* transition, and a peak at 291 eV associated with the 1s-σ* transition.[20] However, clear

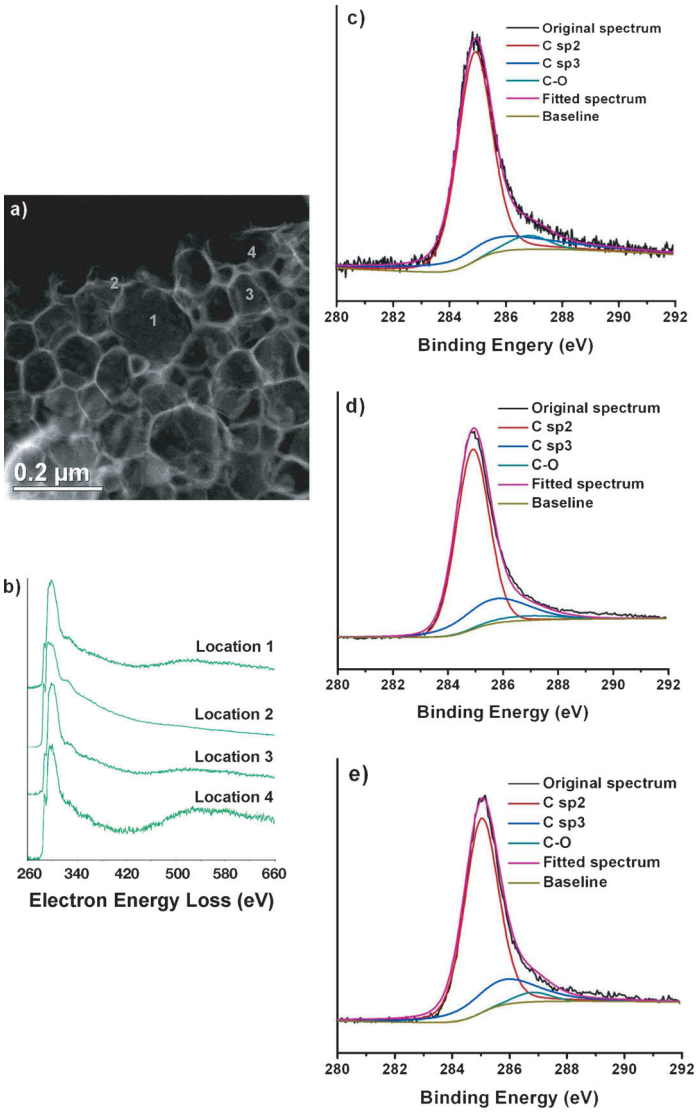

Figure 3. EELS and XPS spectra for honeycomb-structured graphene (HSG). a) High-angle annular dark field (HAADF) image and b) EELS at locations 1–4 of (a) for HSG-48 h; spectra vertically offset for clarity. c) XPS for HSG-12 h, d) XPS for HSG-24 h, and e) XPS for HSG-48 h.

differences in K-edge peaks at 532 eV (associated with oxygen groups[21]) can be observed for different locations, namely, a large oxygen K-edge peak at 532 eV occurs at location 4, a small oxygen K-edge peak at locations 1 and 3, and no oxygen K-edge at location 2. This indicates that HSG sheets contain oxygen groups, which are heterogeneously distributed. The content of the sp^2 and sp^3 bonded carbon as well as oxygen groups was evaluated by X-ray photoelectron spectroscopy (XPS). As shown in Figure 3 c–e, the deconvolution of the C1 s peak revealed three components centered at 284.9, 285.7, and 286.8 eV, which would be associated with sp^2 carbon atoms, sp^3 carbon atoms, and O-C-O groups.[22] The main component is sp^2 bonded carbon (72.6–74.8 %), whereas sp^3 carbon (21.7–22.3 %) and oxygen groups (3.5–5 %) constitute a small part of graphene sheets. This is consistent with the energy dispersive spectroscopy (EDS) analysis that showed 94.6–97.5 % carbon and 2.5–5.4 % oxygen in HSG

(Table S1). Furthermore, with increasing synthesis time for HSG, the content of sp^2 bonded C increases, whereas sp^3 bonded C and the C–O groups decrease.

Raman spectroscopy has been widely exploited to reveal the defect structure of carbon materials with characteristic peaks at approximately 1350 cm^{-1} (D band corresponding to the breathing mode of aromatic rings with dangling bonds) and 1580 cm^{-1} (G band associated with the bond stretching of sp^2 carbon pairs).[23] The Raman spectra of HSG exhibit an clear G peak at around 1580 cm^{-1}, providing evidence of an sp^2 bonded carbon (Figure 4a). There is also a D peak with comparable intensity to the G peak, indicating structural defects caused by oxygen-functional groups.[24,25] This is consistent with the XPS results (Figure 3c–e). Furthermore, sheet resistance of the 20 μm HSG film on bare glass is 3.4 kΩ/sq for HSG-12 h, 1.6 kΩ/sq for HSG-24 h, and 0.45 kΩ/sq for HSG-48 h (note: HSG-12, 24, or 48 h denotes HSG synthesized with reaction time of 12, 24, or 48 h). In contrast, CEG (graphene synthesized by chemical exfoliation of graphite) has a large sheet resistance (64 kΩ/sq). These results indicate that HSGs have a much higher conductivity than CEG. Therefore, the structural defects and the high conductivity of HSG offer unique opportunities for its applications related to energy conversion and storage.

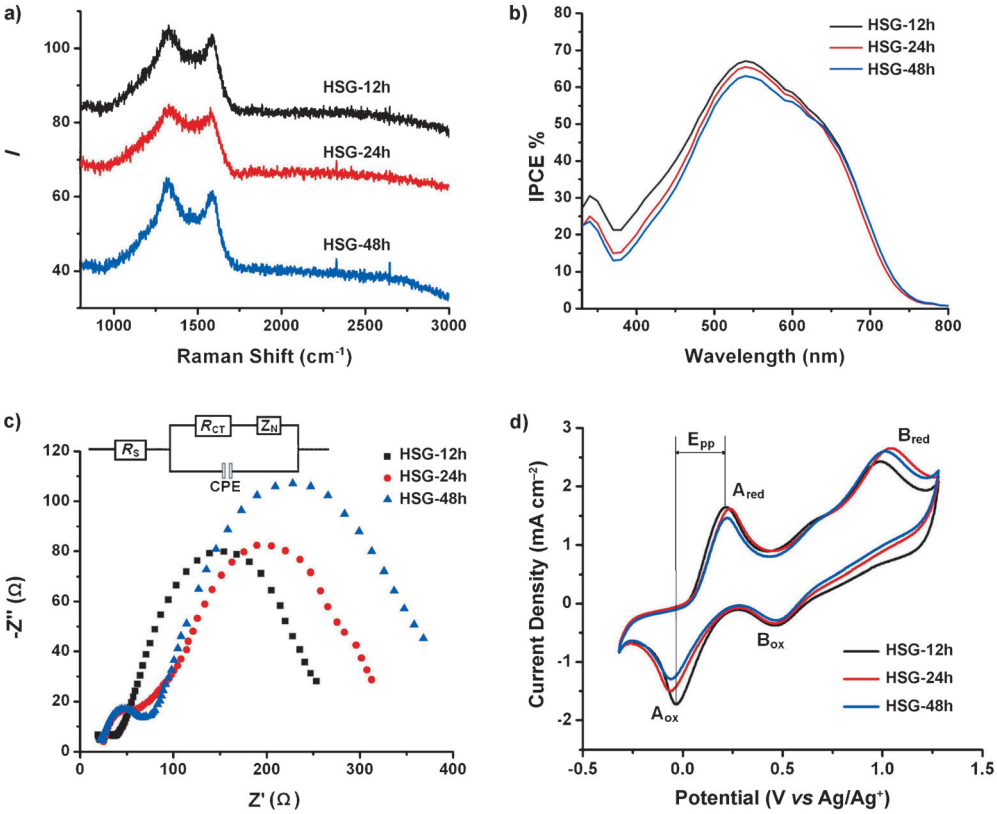

Figure 4. Raman and electrochemical characterizations of honeycomb-structured graphene (HSG). a) Raman spectra, b) IPCE of DSSCs with HSG counter electrodes, c) EIS of DSSCs with HSG counter electrodes, Inset: the corresponding circuit model. d) CV curves of HSG electrodes. (A_{ox} and A_{red} peaks are assigned to a redox reaction between I_3^-/I^-, B_{ox} and B_{red} peaks to a redox reaction between I_2/I_3^-).

The dye-sensitized solar cell (DSSC) is a third-generation photovoltaic device.[26] As an important component in DSSCs, a counter electrode (CE) plays a role in the reduction of I_3^- to I^- for iodine-based electrolytes. An ideal CE material should have a small sheet resistance, high catalytic activity, and a low cost. Currently, platinum-loaded conducting glass is widely exploited as a CE for DSSCs. However, the high cost of platinum would limit its application. This problem has motivated the development of carbon-based CEs.[27–29] Herein, we employed HSG without any conductive polymer as a CE for DSSCs. The photoelectrode of the DSSCs is N719 dye sensitized TiO_2 film on fluorine-doped tin oxide (FTO) glass plate, and the electrolyte is I_3^-/I^- based liquid. The photovoltaic performance of the DSSCs is summarized in Table 1. The DSSC with HSG-12 h CE exhibited the best performance with the short-circuit current density (J_{sc}) of 27.2 mA cm^{-2}, open-circuit voltage (V_{oc}) of 0.773 V, fill factor (FF) of 0.371, and power conversion efficiency (η) of 7.8% under illumination of AM1.5 simulated sunlight with power density of 100 mW cm^{-2}. This efficiency is 10-times higher than that (0.64%) of the DSSC with a CEG-based CE. Furthermore, it is even comparable to that (8%) of a Pt-based DSSC. However, when the synthesis time increased from 12 to 48 h, the efficiency of the DSSC with a HSG CE decreased from 7.8 to 6.3%. The relationship is further supported by incident photon to charge carrier efficiency (IPCE) spectra (Figure 4b). It is established that two critical factors (electrical conductivity and catalytic activity) determine CE performance for DSSCs, namely, the larger the conductivity and the catalytic activity, the higher the energy conversion

Table 1: Photovoltaic performance and electrochemical characteristics of DSSCs.

CE[a]	J_{sc} [mA cm^2]	V_{oc} [V]	FF	η [%]	R_s [Ω]	R_{ct} [Ω]	Z_N [Ω]
HSG-12 h	27.2	0.773	0.371	7.80	24	20	220
HSG-24 h	26	0.774	0.325	6.53	25	35	265
HSG-48 h	26	0.773	0.314	6.30	24	45	310
CEG	6.48	0.785	0.127	0.64	27	2500	10^4

[a] CE: counter electrode; HSG-12 h, HSG-24 h, and HSG-48 h: honeycomb-structured graphene synthesized for 12, 24, and 48 h; CEG: Graphene synthesized by chemical exfoliation of graphite.

efficiency is. However, when HSG synthesis time increased from 12 to 48 h, HSG conductivity increased (which is reflected by decrease in its sheet resistance from 3.4 to 0.45 kΩ/sq), whereas the efficiency of HSG-based DSSC decreased. This indicates that the decrease in efficiency with increasing HSG synthesis time is not due to the variation of HSG conductivity. It has been recognized that defects in graphene sheets are the active sites for the catalytic reduction of I_3^- to I^- at the CE.[30] Furthermore, it was suggested that the defects arising from nitrogen-doping could play a catalytic role.[31] Similarly, the existence of oxygen in HSG sheets could generate the defects as catalytic sites (Figure 3c–e). The XPS results showed that the increase in HSG synthesis time decreased the number of oxygen-containing groups, indicating a decrease in structural defects and thus the decrease in catalytic activity. Therefore, the decrease in catalytic activity with increasing HSG synthesis time would be responsible for the decrease in HSG-based DSSC efficiency. This notion is further supported by electrochemical impedance spectroscopy (EIS) measurements (Figure 4c). The EIS curves were fitted by equivalent circuit model with Z-view software (Figure 4c) and summarized in Table 1. The first semicircle corresponds to charge-transfer resistance (R_{ct}) at CE/electrolyte interface, which changes inversely with catalytic ability of CEs for the reduction of I_3^- to I^-, while the semicircle in lower frequency region is attributed to Nernst diffusion process (Z_N).[32] As the three HSG counter electrodes have nearly the same value of R_s, the effect of R_s on photovoltaic performance can be neglected. The value of R_{ct} increases in the order of HSG-12 h (20 Ω) < HSG-24 h (35 Ω) < HSG-48 h (45 Ω), which is inverse to the order of electrocatalytic activity. Although HSG-12 h has the highest intrinsic sheet resistance, it exhibits the lowest R_{ct} at the interface owing to it having the highest catalytic activity. Furthermore, the DSSC with a CEG CE has a very large R_{ct} (2500 Ω), indicating its very low catalytic activity and thus explains why its power conversion efficiency is negligible.

Cyclic voltammetry (CV) curves were obtained for three HSG CEs, which show two pairs of oxidation and reduction peaks (Figure 4d). Since a DSSC CE mainly catalyzes the reduction of I_3^- to I^-, which can be evaluated by the peak current density and the peak-to-peak separation (E_{pp}) of A_{ox} and A_{red} peaks, namely, the higher the peak current density and the lower the E_{pp} value, the better the catalytic activity is.[33] The HSG-12 h CE showed the highest current density (1.644 mA cm^{-2}) and the lowest E_{pp} (0.246 V) of the three electrodes (Figure 4d), indicating it has the best electrocatalytic activity. This further supports the results of *J-V*, IPCE, and EIS measurements.

In summary, a novel approach, which is based on a simple reaction between Li_2O and CO, was exploited to synthesize 3D honeycomb-like structured graphene sheets. Furthermore, the dye-sensitized solar cell with the honeycomb-structured graphene counter electrode gave an energy conversion efficiency as high as 7.8%, which is even comparable to that of DSSCs with an expensive Pt counter electrode. In addition, the honeycomb-structured graphene is promising for applications in energy storage devices, such as batteries and supercapacitors.

Received: April 24, 2013
Revised: June 9, 2013
Published online: July 29, 2013

Keywords: counter electrodes · dye-sensitized solar cells · graphene · honeycomb structure · lithium oxide

[1] K. S. Novoselov, A. K. Geim, S. V. Morozov, D. Jiang, Y. Zhang, S. V. Dubonos, I. V. Grigorieva, A. A. Firsov, *Science* **2004**, *306*, 666 – 669.
[2] R. R. Nair, P. Blake, A. N. Grigorenko, K. S. Novoselov, T. J. Booth, T. Stauber, N. M. R. Peres, A. K. Geim, *Science* **2008**, *320*, 1308.
[3] C. Lee, X. Wei, J. W. Kysar, J. Home, *Science* **2008**, *321*, 385 – 388.
[4] P. Sutter, *Nat. Mater.* **2009**, *8*, 171 – 172.
[5] K. Kim, Y. Zhao, H. Jang, S. Y. Lee, J. M. Kim, K. S. Kim, J.-H. Ahn, P. Kim, J.-Y. Choi, B. H. Hong, *Nature* **2009**, *457*, 706 – 710.
[6] S. Stankovich, D. A. Dikin, R. D. Piner, K. A. Kohlhaas, A. Kleinhammes, Y. Jia, Y. Wu, S. T. Nguyen, R. S. Ruoff, *Carbon* **2007**, *45*, 1558 – 1565.
[7] L. J. Cote, R. Cruz-Silva, J. X. Huang, *J. Am. Chem. Soc.* **2009**, *131*, 11027 – 11032.
[8] Z. Chen, W. Ren, L. Gao, B. Liu, S. Pei, H.-M. Cheng, *Nat. Mater.* **2011**, *10*, 424 – 428.
[9] Y. Zhu, S. Murali, M. D. Stoller, K. J. Ganesh, W. Cai, P. J. Ferreira, A. Pirkle, R. M. Wallace, K. A. Cychosz, M. Thommes, D. Su, E. A. Stach, R. S. Ruoff, *Science* **2011**, *332*, 1537 – 1541.
[10] Z. S. Wu, Y. Sun, Y. Z. Tan, S. Yang, X. Feng, K. Müllen, *J. Am. Chem. Soc.* **2012**, *134*, 19532 – 19535.
[11] Z. S. Wu, S. Yang, Y. Sun, K. Parvez, X. Feng, K. Müllen, *J. Am. Chem. Soc.* **2012**, *134*, 9082 – 9085.
[12] Z. S. Wu, A. Winter, L. Chen, Y. Sun, A. Turchanin, X. L. Feng, K. Müllen, *Adv. Mater.* **2012**, *24*, 5130 – 5135.
[13] W. J. Yu, S. H. Chae, D. Perello, S. Y. Lee, G. H. Han, M. Yun, Y. H. Lee, *ACS Nano* **2010**, *4*, 5480 – 5486.
[14] C. Hu, Y. Zhao, H. Cheng, Y. Wang, Z. Dong, C. Jiang, X. Zhai, L. Jiang, L. Qu, *Nano Lett.* **2012**, *12*, 5879 – 5884.
[15] B. G. Choi, M. H. Yang, W. H. Hong, J. W. Choi, Y. S. Huh, *ACS Nano* **2012**, *6*, 4020 – 4028.
[16] X. Huang, K. Qian, J. Yang, J. Zhang, L. Li, C. Yu, D. Zhao, *Adv. Mater.* **2012**, *24*, 4419 – 4423.
[17] M. C. J. Bradford, M. A. Vannice, *Catal. Rev.* **1999**, *41*, 1 – 42.
[18] J. C. Meyer, A. K. Geim, M. I. Katsnelson, K. S. Novoselov, T. J. Booth, S. Roth, *Nature* **2007**, *446*, 60 – 63.
[19] S. Stankovich, D. A. Dikin, G. H. B. Dommett, K. M. Kohlhaas, E. J. Zimney, E. A. Stach, R. D. Piner, S. T. Nguyen, R. S. Ruoff, *Nature* **2006**, *442*, 282.
[20] P. K. Chu, L. Li, *Mater. Chem. Phys.* **2006**, *96*, 253 – 277.
[21] R. Wirth, *Phys. Chem. Miner.* **1997**, *24*, 561 – 568.
[22] W. Zhang, J. Cui, C. Tao, Y. Wu, Z. Li, L. Ma, Y. Wen, G. Li, *Angew. Chem.* **2009**, *121*, 5978 – 5982; *Angew. Chem. Int. Ed.* **2009**, *48*, 5864 – 5868.
[23] A. C. Ferrari, J. C. Meyer, V. Scardaci, C. Casiraghi, M. Lazzeri, F. Mauri, S. Piscanec, D. Jiang, K. S. Novoselov, S. Roth, A. K. Geim, *Phys. Rev. Lett.* **2006**, *97*, 187401.
[24] K. N. Kudin, B. Ozbas, H. C. Schniepp, R. K. Prud'homme, I. A. Aksay, R. Car, *Nano Lett.* **2008**, *8*, 36 – 41.
[25] J. M. Englert, C. Dotzer, G. Yang, M. Schmid, C. Papp, J. M. Gottfried, H.-P. Steinrück, E. Spiecker, F. Hauke, A. Hirsch, *Nat. Chem.* **2011**, *3*, 279 – 286.
[26] A. Yella, H. W. Lee, H. N. Tsao, C. Yi, A. K. Chandiran, M. K. Nazeeruddin, E. W. Guang Diau, C. Y. Yeh, S. M. Zakeeruddin, M. Grätzel, *Science* **2011**, *334*, 629.
[27] H. Wang, Y. H. Hu, *Energy Environ. Sci.* **2012**, *5*, 8182 – 8188.
[28] L. Kavan, J. H. Yum, M. K. Nazeeruddin, M. Gratzel, *ACS Nano* **2011**, *5*, 9171 – 9178.

[29] H. Choi, H. Kim, S. Hwang, Y. Han, M. Jeon, *J. Mater. Chem.* **2011**, *21*, 7548 – 7551.
[30] J. D. Roy-Mayhew, D. J. Bozym, C. Punckt, I. A. Aksay, *ACS Nano* **2010**, *4*, 6203 – 6211.
[31] Y. Xue, J. Liu, H. Chen, R. Wang, D. Li, J. Qu, L. Dai, *Angew. Chem.* **2012**, *124*, 12290 – 12293; *Angew. Chem. Int. Ed.* **2012**, *51*, 12124 – 12127.
[32] F. Gong, H. Wang, X. Wu, G. Zhou, Z. S. Wang, *J. Am. Chem. Soc.* **2012**, *134*, 10953 – 10958.
[33] R. Bajpai, S. Roy, P. Kumar, P. Bajpai, N. Kulshrestha, J. Rafiee, N. Koratkar, D. S. Misra, *ACS Appl. Mater. Interfaces* **2011**, *3*, 3884 – 3889.

